Journal of Asian Earth Sciences 138 (2017) 399–415

Contents lists available at ScienceDirect

Journal of Asian Earth Sciences

journal homepage: www.elsevier.com/locate/jseaes

Full length Article

Site correction of a high-frequency strong-ground-motion simulation based on an empirical transfer function

Jyun-Yan Huang [a], Kuo-Liang Wen [a,b,*], Che-Min Lin [a], Chun-Hsiang Kuo [a], Chun-Te Chen [c], Shuen-Chiang Chang [b]

[a] National Center for Research on Earthquake Engineering, No. 200, Sec. 3, HsinHai Rd., Taipei City, Taiwan
[b] Department of Earth Sciences, National Central University, No. 300, Zhongda Rd., Zhongli District, Taoyuan City, Taiwan
[c] Institute of Earth Sciences, Academia Sinica, No. 128, Sec. 2, Academia Road, Nangang, Taipei City, Taiwan

ARTICLE INFO

Article history:
Received 29 June 2016
Received in revised form 23 January 2017
Accepted 26 January 2017
Available online 10 February 2017

Keywords:
Empirical transfer function
Stochastic simulation
Site correction
Taipei Basin

ABSTRACT

In this study, an empirical transfer function (ETF), which is the spectrum difference in Fourier amplitude spectra between observed strong ground motion and synthetic motion obtained by a stochastic point-source simulation technique, is constructed for the Taipei Basin, Taiwan. The basis stochastic point-source simulations can be treated as reference rock site conditions in order to consider site effects. The parameters of the stochastic point-source approach related to source and path effects are collected from previous well-verified studies. A database of shallow, small-magnitude earthquakes is selected to construct the ETFs so that the point-source approach for synthetic motions might be more widely applicable. The high-frequency synthetic motion obtained from the ETF procedure is site-corrected in the strong site-response area of the Taipei Basin. The site-response characteristics of the ETF show similar responses as in previous studies, which indicates that the base synthetic model is suitable for the reference rock conditions in the Taipei Basin. The dominant frequency contour corresponds to the shape of the bottom of the geological basement (the top of the Tertiary period), which is the Sungshan formation. Two clear high-amplification areas are identified in the deepest region of the Sungshan formation, as shown by an amplification contour of 0.5 Hz. Meanwhile, a high-amplification area was shifted to the basin's edge, as shown by an amplification contour of 2.0 Hz. Three target earthquakes with different kinds of source conditions, including shallow small-magnitude events, shallow and relatively large-magnitude events, and deep small-magnitude events relative to the ETF database, are tested to verify site correction. The results indicate that ETF-based site correction is effective for shallow earthquakes, even those with higher magnitudes, but is not suitable for deep earthquakes. Finally, one of the most significant shallow large-magnitude earthquakes (the 1999 Chi-Chi earthquake in Taiwan) is verified in this study. A finite fault stochastic simulation technique is applied, owing to the complexity of the fault rupture process for the Chi-Chi earthquake, and the ETF-based site-correction function is multiplied to obtain a precise simulation of high-frequency (up to 10 Hz) strong motions. The high-frequency prediction has good agreement in both time and frequency domain in this study, and the prediction level is the same as that predicted by the site-corrected ground motion prediction equation.

1. Introduction

Reductions of estimation errors for ground motion are important in engineering seismology. In practice, the ground motion prediction equation (GMPE) is applied to target sites. However, as site classification for a given location is typically not sufficiently clear in many regions, the GMPE should first consider rock site attenuation. Using typical estimation methods, basin and sedimentary data are either excluded in order to check the response of a rock outcrop or are not discriminated, and anomalies are explained in terms of site effects (Boore and Joyner, 1982; Douglas, 2003). In recent years, soil site amplification has been highlighted separately for prediction purposes given the site conditions. Jean et al. (2006) constructed a two-phase regression procedure that combines the rock site attenuation equation and a site-dependent ground motion prediction model for different sites in order to incorporate

* Corresponding author at: Department of Earth Sciences, National Central University, No. 300, Zhongda Rd., Zhongli District, Taoyuan City, Taiwan.
E-mail addresses: jyhuang@narlabs.org.tw (J.-Y. Huang), wenkl@earth.ncu.edu.tw (K.-L. Wen), cmlin@narlabs.org.tw (C.-M. Lin), chkuo@ncree.narl.org.tw (C.-H. Kuo), pokayoke69@gmail.com (C.-T. Chen), fcuiii@gmail.com (S.-C. Chang).

http://dx.doi.org/10.1016/j.jseaes.2017.01.035
1367-9120/

a site-correction term in the GMPE. Meanwhile, a global crustal ground motion database was constructed based on the Next Generation Attenuation of Ground Motions Project (NGA) at the Pacific Earthquake Engineering Research Center (PEER, UC, Berkeley). Several unsolved effects in the GMPE were extracted, in which the site classification technique (using the average shear wave velocity up to 30 m in depth, Vs30) was one of the most important criteria for reducing prediction errors (Abrahamson et al., 2008; Boore and Atkinson, 2008; Campbell and Bozorgnia, 2008; Chiou and Youngs, 2008).

As mentioned above, the GMPE is frequently used for different engineering purposes, such as hazard analysis, structural seismic design, and disaster prevention. However, seismologists apply wave propagation theory to one-dimensional, two-dimensional (2D), and three-dimensional (3D) models of subterranean velocity structures to simulate the full waveforms at each target site. Strong site effects induced by sedimentary basins such as the Taipei Basin can already be considered in a 3D simulation, but the reliable frequency band is still lower than 1 Hz, owing to shallow velocity structures not being sufficiently clear. Current techniques, such as the spectral element method and finite difference method cannot achieve the high-frequency (of at least 10 Hz) responses that are mainly induced by site effects (Lee et al., 2008a,b; Miksat et al., 2010).

To realize a high-frequency ground motion simulation, there are two common techniques, namely the empirical green's function (Irikura, 1986; Miyake et al., 2003) and the stochastic ground motion simulation (Boore, 1983, 2003, 2009; Beresnev and Atkinson, 1998a; Motezedian and Atkinson, 2005). The main concept of the former is that only a source scaling relationship between small and large earthquakes is considered if they are located in the same seismogenic source zone. This means that the observed waveform of a small earthquake can be treated as a Green's function and that the response of a large earthquake can be predicted after considering the reliable strong motion generation area (Kurahashi and Irikura, 2011). The simulated results can yield reasonable time histories, as the true phase spectra of small earthquakes are applied initially. However, suitable small earthquakes might not have occurred previously in some seismogenic zones, so the technique might not be applicable to some target sites, such as for the analysis of seismic responses for metropolitan areas of Tokyo or Taipei.

The stochastic ground-motion simulation technique constructs a random-phase waveform and considers the ω^2 source spectrum model (Aki, 1967; Brune, 1970) combined with correction factors for source, path, and site effects. This technique applies a point source and finite-fault simulation, depending on the earthquake magnitude as well as source-site distance. It then predicts the level of strong motion using a spectrum-fitting process in the frequency domain. However, simulated waveforms cannot match the real time histories, because of the random phase setting at the beginning, and only a seismic wave-like envelope function can be applied in the time domain. Nevertheless, they can still produce good agreement in strong motion levels, such as peak ground acceleration (PGA) or the frequency spectrum; hence, it is still useful for producing preliminary evaluations for possible future earthquakes. Therefore, the stochastic ground-motion simulation technique is employed in this study.

Numerous correction factors have been taken into account over the past few decades for stochastic simulations. Each factor has been discovered and solved step-by-step since the discovery of the stochastic simulation technique in the 1980s (Boore, 1983). Site amplification is one of the most important factors, which still needs to be carefully determined for each site, except for some well-studied common factors, such as path attenuation, high-frequency attenuation, geometric spreading, and the crust transfer function. These well-known factors should be adjusted using empirical observation data in different seismogenic regions (Atkinson, 1995; Atkinson and Silva, 1997; Atkinson and Beresnev, 2002; Atkinson and Boore, 1998, 2006; Boore et al., 1992; Chandler et al., 2006; D'Amico et al., 2012; Hung and Kiyomiya, 2013; Sokolov et al., 2000). Most of the site responses used in the stochastic ground-motion simulation technique are simplified and only the rock-like site response is considered. For example, the generic rock site response of Western North America from Boore and Joyner (1997) was used to simulate the 1994 Northridge earthquake (Beresnev and Atkinson, 1998b). Atkinson and Boore (2006) constructed site amplification factors for Eastern North America (ENA) for site A (where Vs30 > 1500 m/s) and the B C boundary (Vs30 = 760 m/s) based on empirical data from Siddiqqi and Atkinson (2002) and Frankel et al. (1996). A series of site effect studies in the frequency domain for Taiwan were conducted based on spectral differences between synthetic very hard rock (VHR) and observed soil records, as a traditional reference rock site cannot be easily applied to a spectral ratio calculation in many cases (Sokolov et al., 2000; Sokolov et al., 2001, 2003, 2009).

The Taipei Basin, Taiwan, has been greatly influenced by site effects during an earthquake (Fletcher and Wen, 2005; Wen et al., 1995; Wen and Peng, 1998). The basin is triangular and the subsurface structure is deeper on the west side than on the east side. The deepest geological basement (top of the Tertiary period) is located at approximately 680 m and the deepest engineering basement (the bottom of the Sungshan formation) is approximately 100 m (Wang et al., 2004). The engineering basement is the boundary of shear-wave velocity within 300–700 m/s, and the majority of short-period site amplification of seismic waves will be affected in the topmost shallow subsurface layer (NIED, 2009; Irikura and Miyake, 2011). The Sungshan formation was found to be composed of unconsolidated sand, silt, and clay (Wang et al., 2004) and related to the main amplification of PGA and the dominant frequency during earthquakes (Wen et al., 1995; Wen and Peng, 1998).

The issue of seismic disaster prevention within the basin is quite important, as ground motions have been enlarged in historical earthquakes. For example, in the case of the Chi-Chi earthquake in 1999, even though the epicenter was 100 km away, damage was caused to over 450 houses in the Taipei Basin (Tsai et al., 2000). The March 31, 2002, M_L-6.8 earthquake resulted in five deaths and injuries to over 250 people in the basin; although the epicentral distance was also >100 km, more damage was caused in the basin than in the nearby regions (Chen, 2003). Therefore, in this study, site correction was performed for the Taipei Basin by applying the stochastic simulation in order to reduce the uncertainties in high-frequency simulation.

2. Methodology for stochastic simulation

The central concept of the stochastic ground-motion simulation technique is that a seismic source can be treated as a circular rupture process and propagated forward to target stations. Thus, the source spectrum should correspond to a ω^2 model and, as the real seismic phase cannot be easily predicted, a random phase was used for this technique.

The point source method mentioned above is typically used to deal with small earthquakes. On the other hand, for some complex rupture earthquakes, the finite fault model should be taken into consideration. A rectangular fault composed of several point source

subfaults was constructed in the finite fault model and synthetic waveforms from each subfault were superposed after considering the time delay from the rupture velocity and propagation velocity. The detailed methodology will be described in the following paragraphs.

The stochastic point source simulation was constructed based on the ω^2 source model (Boore, 1983; Stochastic Model Simulation, SMSIM). First, random-phase white noise with a zero-mean time history was established and multiplied with a seismic wave–like envelope function. Second, the time history was Fourier transformed to the frequency domain and multiplied by a specified spectrum. Finally, the spectrum was transformed back to the time domain to complete the simulation.

The specified spectrum should be considered as the product of a theoretical source term (E), a path term (P), and a site term (G). The theoretical Fourier amplitude spectrum of ground motion record (Y) is arranged as follows (Boore, 2003):

$$Y(M_0,R,f) = E(M_0,f)P(R,f)G(f)I(f), \tag{1}$$

where $I(f)$ is an instrumental control term and M_0 is the seismic moment. The source term E can be defined as:

$$E(M_0,f) = CM_0S(M_0,f), \text{ where} \tag{2}$$

$$S(M_0,f) = \frac{1}{1+(f/f_0)^2}, \tag{3}$$

$$f_0 = 4.9\times10^6\beta(\Delta\sigma/M_0)^{1/3}, \text{ and} \tag{4}$$

$$C = \frac{R_{\theta\phi}\cdot V\cdot F}{4\pi\rho\beta^3R_0}. \tag{5}$$

Here, C is a constant, f is frequency, f_0 is the corner frequency (in Hz), $\Delta\sigma$ denotes the stress drop (in bars), β denotes the shear wave velocity, and ρ is density. The units of M_0 are dynes per centimeter and units for β are kilometers per second (Brune, 1970). In this equation, V is an index to divide seismic energy into two horizontal components; it is typically $1/\sqrt{2} = 0.707$. Next, F is a factor representing the effect of the free surface for correcting SH waves; it is normally 2. Finally, R_0 is the reference distance and it is normally set as 1 km. Equation $S(M_0,f)$ follows the ω^2 source model from Aki (1967) and Brune (1970).

The path term P is multiplied by the geometrical spreading term and the quality factor as follows:

$$P(R,f) = Z(R)exp[-\pi fR/Q(f)c_Q], \tag{6}$$

where c_Q is the shear wave velocity when calculating the frequency-dependent quality factor $Q(f)$. The geometric spreading term $Z(R)$ denotes the attenuation relation with distance, which is:

$$Z(R) = \begin{cases} \frac{R_0}{R} & R \leqslant R_1 \\ Z(R_1)\left(\frac{R_1}{R}\right)^{P_1} & R_1 \leqslant R \leqslant R_2 \\ \vdots & \\ \vdots & \\ Z(R_n)\left(\frac{R_n}{R}\right)^{P_n} & R_n \leqslant R \end{cases}. \tag{7}$$

Distance R is normally the closest distance to the fault plane here, and $Z(Rn)$ and P_n are attenuation indexes for different distance groups.

The site terms include amplification $A(f)$ and attenuation $D(f)$, which are combined as:

$$G(f) = A(f)D(f). \tag{8}$$

The amplification factor mentioned here is normally related to the seismic source somewhat the impedance from depth of source to surface but not related to local site effects. It is a crust amplification effect and it can be considered as the response from a layered structure constructed in a half-space simulation. Atkinson and Boore (2006) considered the amplification factor of the ENA site A as a crust amplification effect and this study adopted the same setting. The responses of the attenuation phenomenon related to the site term are usually of a high frequency. The high-frequency acceleration spectrum from the observation records indicated a significant drop that could be treated as a high cut filter. Hanks (1982) mentioned the high-frequency attenuation index f_{MAX}, which showed that path attenuation could not respond at this frequency and this parameter was related to the near-surface site conditions. Meanwhile, Anderson and Hough (1984) showed that an exponential form could better describe high-frequency attenuation and gave the equation as follows:

$$D(f) = e^{-\pi\kappa_0 f}, \tag{9}$$

where κ_0 is the local high-frequency attenuation characteristic of a target site when the distance is equal to reference distance (usually set as 1 km, with units in seconds). A smaller κ_0 means a harder site condition (Boore and Joyner, 1997), and this value would vary for different regions, even for the same site conditions (Atkinson, 1996; Ktenidou et al., 2014; Sun et al., 2013). In this study, Eq. (9) was used for the stochastic simulation.

The instrumental control term $I(f)$ can be expressed as follows:

$$I(f) = (2\pi fi)^n, \tag{10}$$

where $i = \sqrt{-1}$, and n is equal to 0, 1, and 2 when related to displacement, velocity, and acceleration, respectively.

Discussed above was the site-specific spectrum describing ground motion in the frequency domain. The next step of the stochastic simulation is constructing a random-phase signal in the time domain and multiplying it by a seismic wave–like shaping window. An exponential window was commonly suggested in previous studies (Boore, 1983, 2003); the formula used was given by Saragoni and Hart (1974) as follows:

$$w(t;\epsilon,\eta,t_\eta) = a(t/t_\eta)^b exp(-c(t/t_\eta)), \text{ where} \tag{11}$$

$$b = -(\epsilon\ln\eta)/[1+\epsilon(\ln\epsilon-1)], \tag{12}$$

$$c = b/\epsilon, \text{ and} \tag{13}$$

$$a = (exp(1)/\epsilon)^b. \tag{14}$$

Here, indexes a, b, and c will determine that the largest level of envelop will occur at time $t = \epsilon\times t_\eta$ and that $w(t) = \eta$ when time $t = t_\eta$ ($\epsilon = 0.2$ and $\eta = 0.05$ were suggested by Boore, 2003). The total simulated time t_η proportional to the summation of the source duration T_d and the path duration T_p can be expressed as follows:

$$t_\eta = d\times(T_d+T_p), \tag{15}$$

where d is a constant and set as 2 (Boore, 2003) here. Furthermore, the source duration and path duration may vary for different seismogenic regions. Boore and Thompson (2014) revised the calculation of the path duration term and, from the residual between prediction and observation, reported that site duration should be taken into account except at rock site stations. Lee et al. (2015) defined the effective shaking duration (ESD, denoted as τ_{ESD} in Eq. (16), below) from Taiwan's strong motion data and constructed a duration equation from the regression process. The ESD considers the duration source, duration path (related to hypocentral distance), and duration site (related to Vs30). The equation is as follows:

Table 1
Parameters for the stochastic simulation.

Shear wave velocity (β)	3.6 km/s
Density (ρ)	2.8gm/cm^3
Geometric spreading $\frac{1}{R^b}$: b =	1.0 (1–50 km) 0.0(50–170 km) 0.5(>170 km)
Quality factor (Q)	Zone ST: 80f$^{0.9}$ Zone SO: 120f$^{0.8}$ Zone DT: 60f$^{1.0}$
High frequency attenuation (κ)	0.05 s
Crust amplification factor	Transfer function of ENA site A (ENA-A)
Magnitude transform equation	$M_L = 0.961Mw + 0.338 + -0.256$, $M_L < 6.0$ $M_L = 5.115 * (\ln(Mw)) - 3.131 + -0.379$, $M_L \geqq 6.0$
Stress drop (bar)	60, Mw < 5.5; 80, 5.5 ≦ Mw < 6.5 90, 6.5 ≦ Mw, including 1999 Chi-Chi Mw 7.6 earthquake

$$\log \tau_{ESD} = \log \left[\frac{\left(\frac{exp[1.1538+1.3273(M_L-5.57)]}{10^{1.5M_L+16.05}} \right)^{-1/3}}{4.9 \times 10^6 \beta} \right] + (-0.0011) \cdot r_{hyp} + (-0.0004) \cdot V_s30 + 0.3038 \quad (16)$$

where M_L is the local magnitude and r_{hyp} is the hypocentral distance. Eqs. (15) and (16) are combined to suit the situation in Taiwan in this study, as follows:

$$t_\eta = d \times (\tau_{ESD}), \quad (17)$$

which means the ESD is substituted for the calculation of source duration and path duration for the case of Taiwan here.

Therefore, disastrous earthquakes typically result from larger magnitude and complex rupture sources. Thus, point sources might not be suitable for describing the extended earthquake source in a stochastic simulation. Beresnev and Atkinson (1997, 1998a) reported that the fault plane of a target earthquake could be divided into several rectangular subfaults and that each of them could be treated as a circular point source, as was mentioned earlier in this section. The time delay of each subfault was considered according to the relationship between rupture speed and shear wave velocity within each fault plane. For the target site, synthetic waves of each subfault would be superposed after considering the time delay in order to obtain the whole response of the earthquake. The source time of each subfault is related to the characteristics and direction of the rupture. Each point source is triggered when the seismic wave propagates across the center. The time delay t_c can be defined as follows (Irikura, 1983):

$$t_c = \frac{R}{\beta} + \frac{\sqrt{\Delta x^2 + \Delta y^2}}{V_r}, \quad (18)$$

where R is the distance from the center of a subfault to a target station, Δx and Δy are distances from the center of a subfault to the earthquake source, and V_r is the rupture velocity and is equal to $0.8 \times \beta$. According to the conservation of energy law, the seismic moment should be distributed equally to each subfault. The equation of seismic moment of each subfault (m_0) can be given as (Beresnev and Atkinson, 1998a):

$$m_0 = \frac{M_0}{N}, \quad (19)$$

where N is the number of subfaults. Beresnev and Atkinson (1997) also considered slip distribution on the whole fault plane and

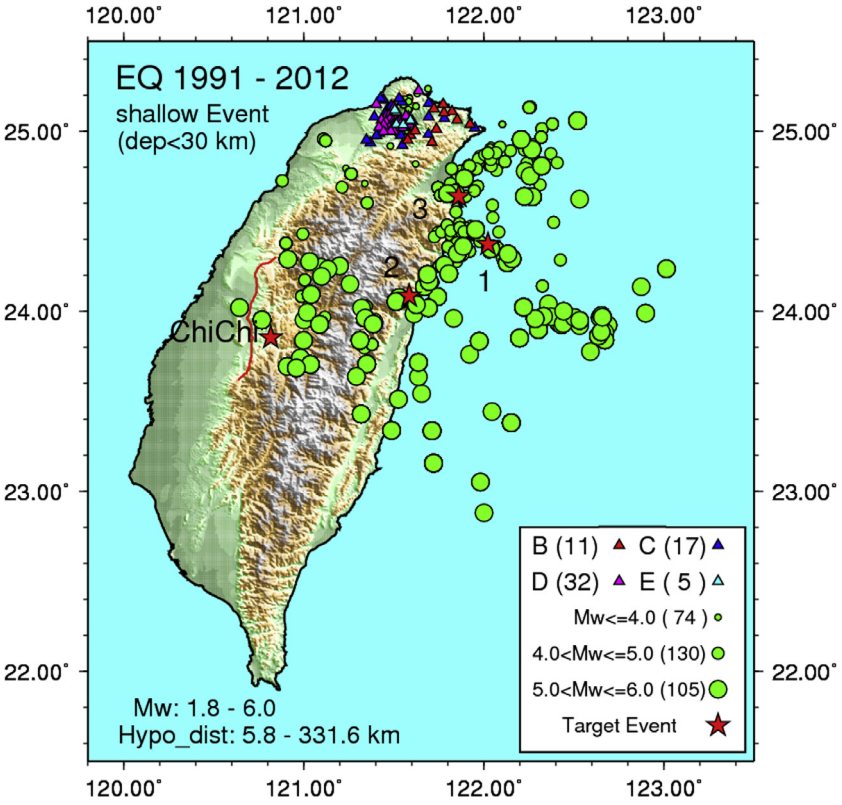

Fig. 1. Shallow earthquake data selected from the TSMIP database in this study. Triangles denote strong motion stations. Site classifications follow the results of P-S logging measurements (Kuo et al., 2012). Circles denote epicenters and magnitudes of earthquakes. Red stars denote target earthquakes used to verify the ETFs constructed in this study. Values in brackets are the corresponding numbers of stations and earthquakes. The red line indicates the surface rupture during the 1999 Chi-Chi earthquake. (For interpretation of the references to colour in this figure legend, the reader is referred to the web version of this article.)

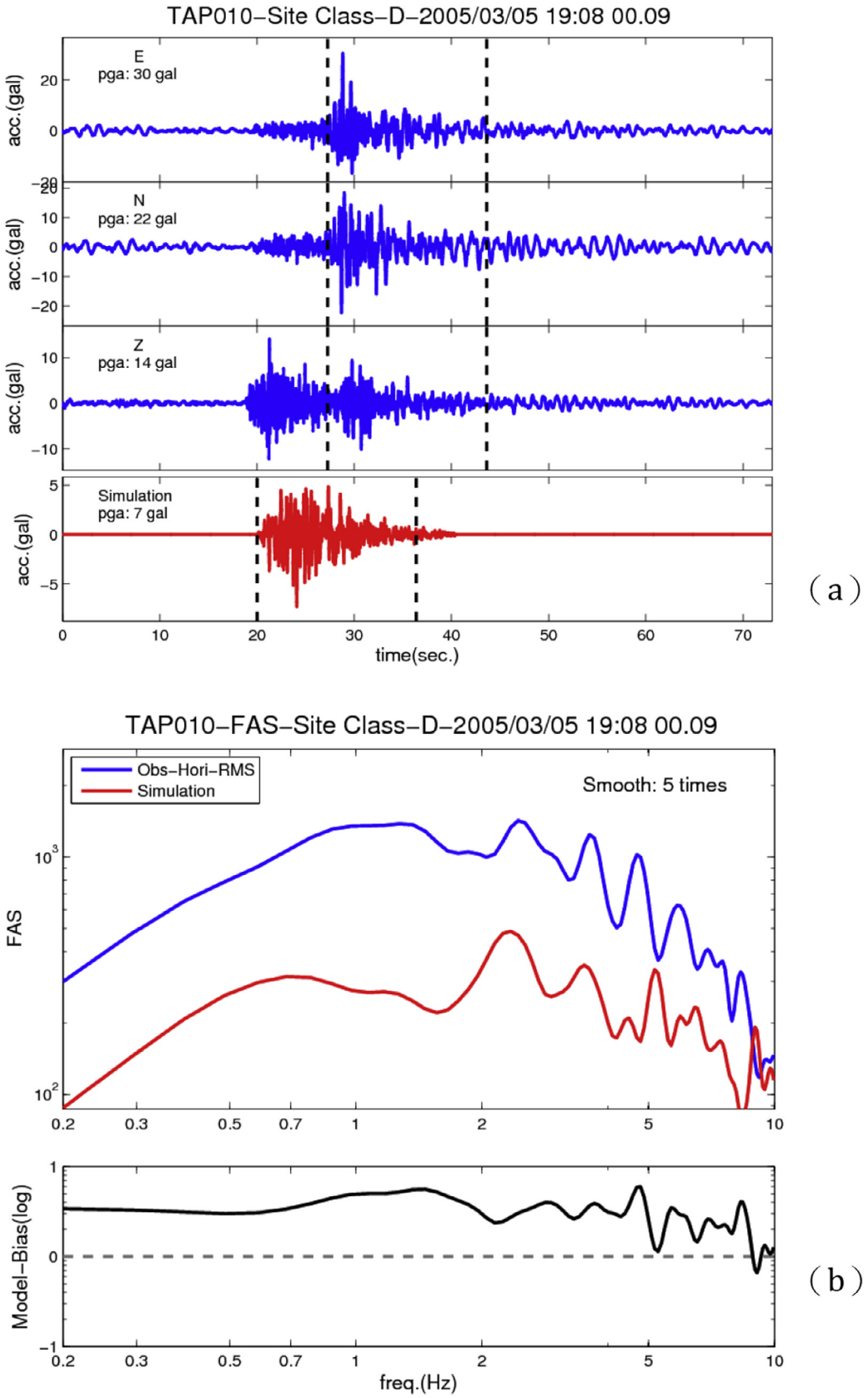

Fig. 2. Example waveforms for calculating model bias from a shear wave window. The records were from station TAP010 during the March 5, 2005 earthquake. (a) From top to bottom are the time histories of the east–west, north–south, vertical, and simulated horizontal components, respectively. The vertical component was only for checking the shear wave window, but it was not used in the ETF calculation. (b) The blue line is the Fourier spectrum from the root-mean-square of two horizontal shear wave windows, the red line is from a simulated window, and the black line is the model bias of observation divided to simulated spectrums. (For interpretation of the references to colour in this figure legend, the reader is referred to the web version of this article.)

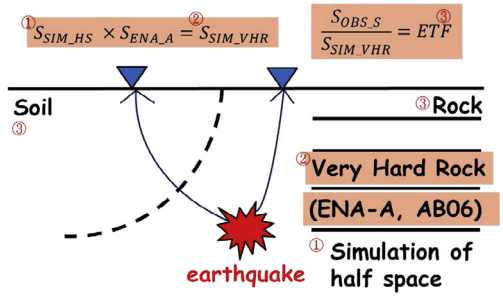

Fig. 3. Flow chart for construction of the ETF for a rock or soil site. The dotted line shows where the sediment basin effect was considered in ETF construction; however, the simulation will only consider the non-basin rock spectrum and multiplies the ETF as a site effect. S denotes the frequency spectrum, SIM_HS is the half-space simulation, "ENA_A, AB06" is the crust amplification following Atkinson and Boore (2006), SIM_VHR is the spectra in VHR conditions, and OBS_S is the observed spectra.

indicated that the total slip value n_s for whole fault plane could be defined as follows:

$$n_s = \frac{M_0}{Nm_0}. \tag{20}$$

If n_s is assumed to be normalized as 1, then the proportion of slip rate at each subfault (proportional weights to n_s) can be considered a relative slip distribution model in the stochastic simulation. Which could also explained as the released seismic energy was proportionally distributed to each subsources.

3. Parameter settings for the stochastic simulation

At the beginning of the 21st century, Sokolov et al. (2000) collated previous studies about the basic parameters needed in the Taiwan region for a stochastic simulation. The parameters used in this study are as follows.

(1) Shear wave velocity and density of crust: $\beta = 3.6$ km/s and $\rho = 2.8$ gm/cm^3 (Sokolov et al., 2009).

(2) Geometric spreading (Eq. (7)): Several studies (Sokolov, 2000; Sokolov et al., 2001, 2003, 2006, 2009) selected the same values for three different situations with gap distances equal to 50 and 170 km and P_n equal to −1.0, 0, and −0.5.

(3) Quality factor ($Q(f)$ in Eq. (6)): Wang (1993) reviewed previous studies of the Q value in Taiwan and mentioned that regional differences are significant, especially in northeastern Taiwan and in deep Taiwan. Tsai (1997) used the attenuation relation given by Chen et al. (1989) for Taiwan to discuss the relationship with source scaling. Roumelioti and Beresnev (2003) have also followed the attenuation relation of Chen et al. (1989) for stochastic finite-fault simulation to discuss soil nonlinearity during 1999 Chi-Chi Taiwan earthquake. Sokolov et al. (2006, 2009) referred to these studies and divided the whole of Taiwan into three regions with different Q values as follows:

$$\begin{cases} Zone\ ST : 80f^{0.9} \\ Zone\ SO : 120f^{0.8} \\ Zone\ DT : 60f^{1.0} \end{cases}, \tag{21}$$

where ST stands for shallow Taiwan, SO for shallow offshore, and DT for deep Taiwan. In this study, 30 km was selected to distinguish between a shallow or deep earthquake.

(4) High-frequency attenuation factor (κ_0 in Eq. (9)): Boore and Joyner (1997) reported $\kappa_0 = 0.04$ s for a VHR site. Sokolov et al. (2009) compared spectral differences in the Taipei Basin and suggested $\kappa_0 = 0.05$ s, which was used in this study.

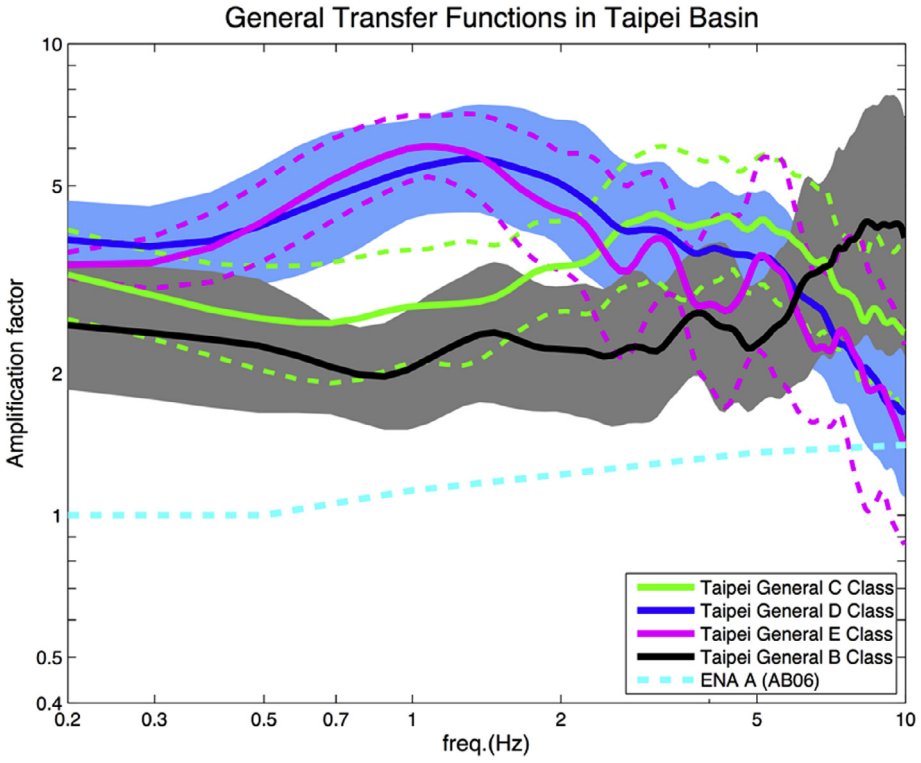

Fig. 4. General ETFs in the Taipei Basin from different site classes. Solid lines are the average ETFs, the thin dashed lines are the standard deviations, and the bold dashed lines are the responses of VHR from Eastern North America (Atkinson and Boore, 2006).

(5) Crust amplification function: Atkinson and Boore (2006) defined the frequency-dependent amplification function for a site A station in ENA. As Taiwan lacks a site A station, in this study the crust amplification function was applied for VHR.

(6) Magnitude transfer equation: As the original catalog from the Central Weather Bureau used M_L but M_w should be used in the stochastic simulation, two-step regression formulas from Cheng et al. (2010) were used:

$$\begin{cases} M_L = 0.961M_w + 0.338 \pm 0.256, & M_L \leqslant 6.0 \\ M_L = 5.115 \times \ln M_w - 3.131 \pm 0.379, & M_L \geqslant 5.5 \end{cases}. \quad (22)$$

These two regression lines overlap when M_L is equal to 5.5 to 6.0.

(7) Stress drop ($\Delta\sigma$ in Eq. (4)): Mayeda and Malagnini (2009) indicated that the stress drop should lie between 5 and 80 bars using Mw 4.7–7.6 data recorded from a broadband array in Taiwan for a seismology network (BATS). D'Amico et al. (2012) employed more data and indicated that the stress drop will not vary significantly with magnitude, which conforms to the self-similarity of an earthquake source (Aki, 1967). The equations used in this study are modified as follows:

$$\begin{cases} M_w < 5.5, & \Delta\sigma = 60\ Bar \\ 5.5 \leqslant M_w < 6.5, & \Delta\sigma = 80\ Bar \\ 6.5 \leqslant M_w, & \Delta\sigma = 90\ Bar \end{cases}. \quad (23)$$

The abovementioned parameters used in this study are listed in Table 1.

4. Construction of the empirical transfer function

Site effects within the Taipei Basin cannot be easily classified from the results of theoretical analysis alone. The 2D or 3D basin response from observation data may also be required. In this study, the ETF is calculated from the spectral ratio of observations with respect to stochastic synthetic motions that do not include the basin structure. The average spectral ratios involve the abovementioned 2D or 3D responses at each station, which are used to produce a site correction function for each station.

Strong motion data were selected for the stations within the Taipei Basin (Fig. 1) from the database of the Taiwan Strong Motion Instrumentation Program (TSMIP) (Tsai and Lee, 2005), within a time span from of 1991 to 2012. As shallow-disastrous earthquakes are a priority for people, the ETF was first constructed from shallow earthquakes. As shown in Fig. 1, 309 earthquakes with focal depths less than 30 km and magnitudes ranging from 1.8 to 6.0 were selected for the earthquake database in order to easily apply the point-source approach for a large number of records. Sokolov et al. (2009) found a significant difference between the site responses of shallow and deep earthquakes in the Taipei Basin, which was found to be due to different angles of incidence of seismic waves moving toward the basin edge. The target earthquake selected for verifying our simulation was the 1999 Chi-Chi earthquake in Taiwan. Only shallow ETF calculation was considered in this study.

The method of constructing the ETF involves two stages. In the first stage, the simulated stochastic point sources of all the earthquakes in the database are included in a half space and the response of a layered structure (the fifth step of the "Parameter Settings for the Stochastic Simulation" section) for each individual

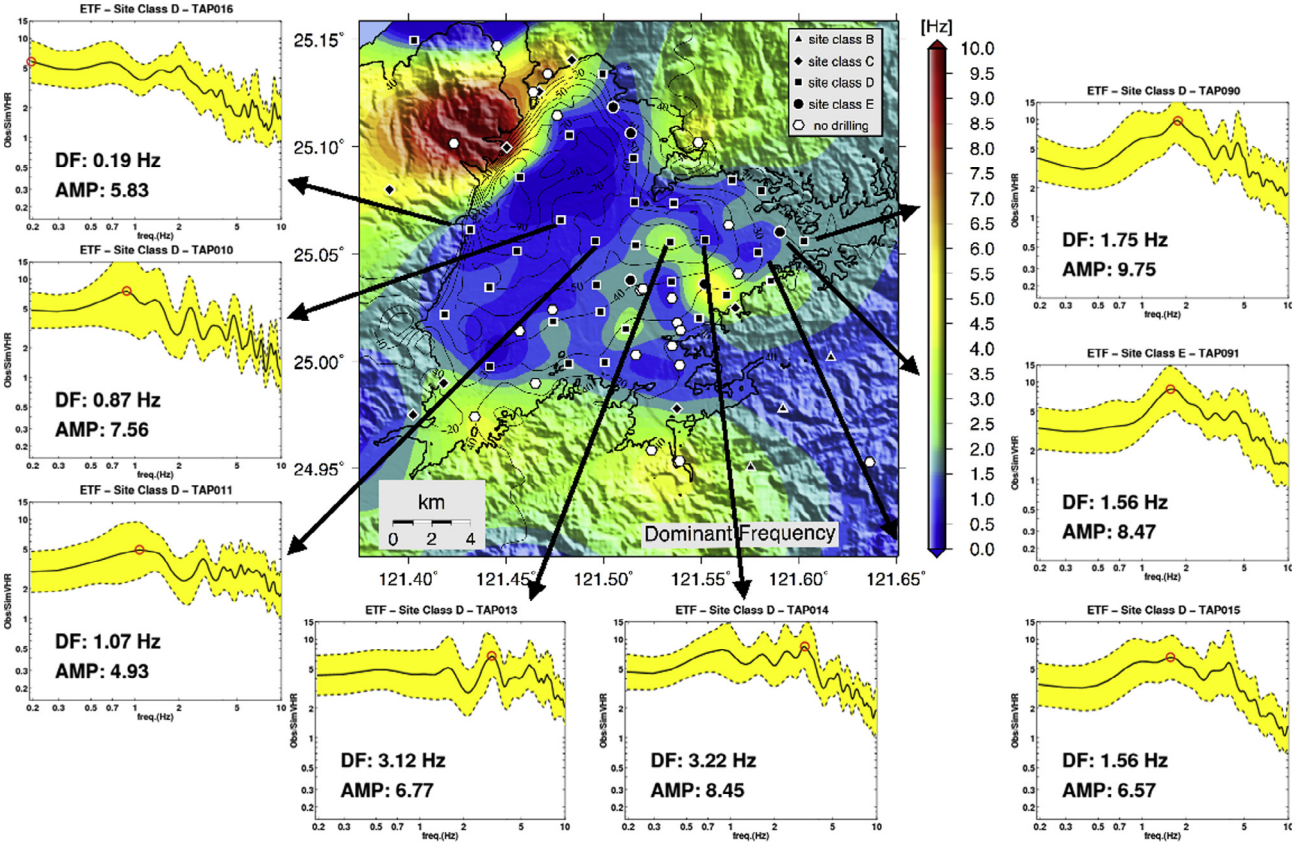

Fig. 5. Contour plot of dominant frequencies in the Taipei Basin from the ETFs of each station. The contour lines show the depth of the bottom of the Sungshan formation according to seismic reflection measurements (redrawn from Wang et al., 2004). Individual ETFs of several stations of a cross-section line across the basin are also shown, DF means dominant frequency and AMP means amplification value of dominant frequency.

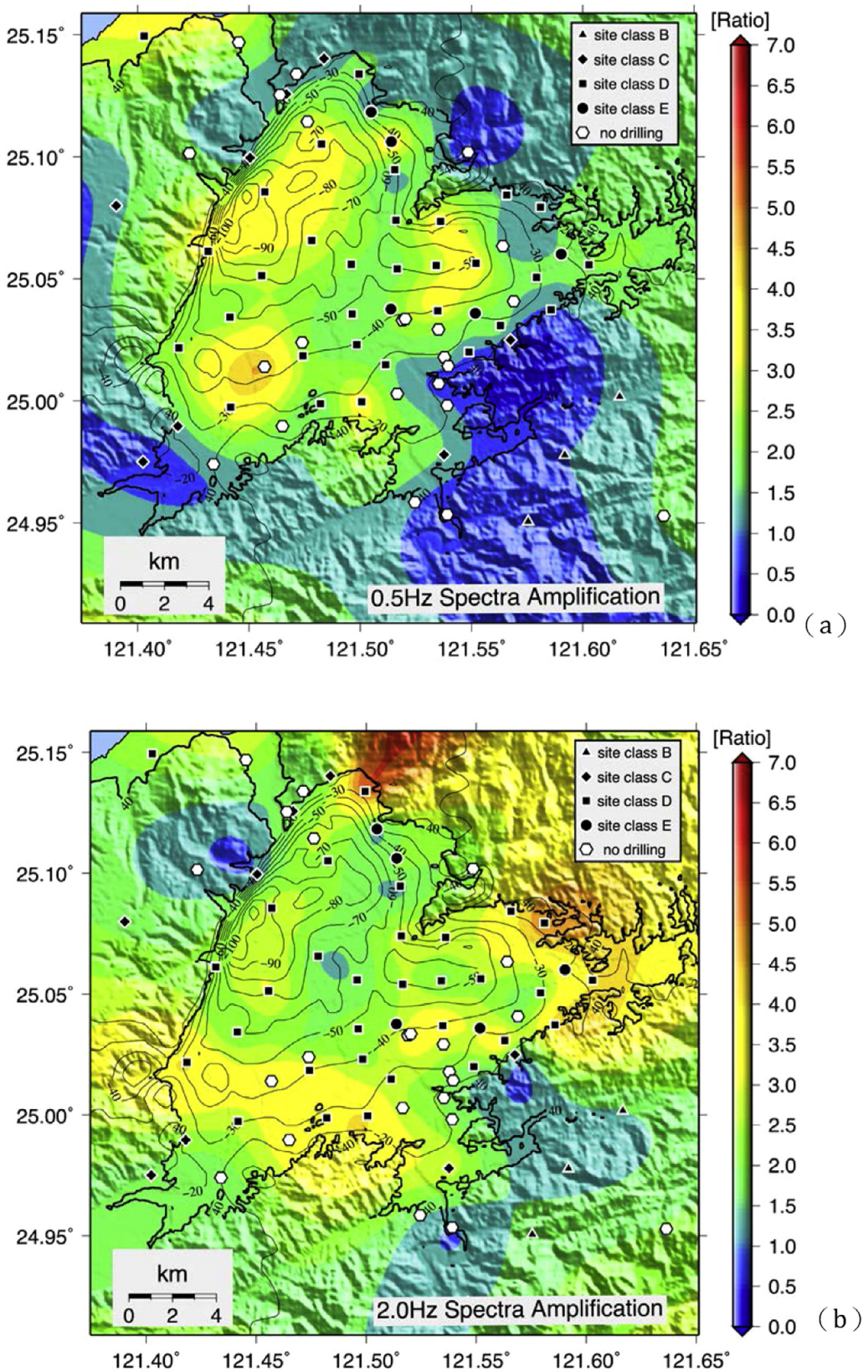

Fig. 6. Contour maps of the amplification of the ETF at (a) 0.5 Hz and (b) 2.0 Hz in the Taipei Basin area. The contour lines show the depth of the bottom of Sungshan formation according to seismic reflection measurements (redrawn from Wang et al., 2004).

station is added in order to extend the simulated spectrum into VHR. In the second stage, the spectrum is classified in terms of shear wave windows of observation and simulation (Fig. 2) to obtain the response between the site itself and VHR. Finally, averaging the spectrum ratios (Model Bias in Fig. 2) of small earthquakes will complete the construction of the ETF (sketch map

shown in Fig. 3; example ETF shown in Fig. 5). Fig. 4 shows the average ETFs for different site classes from the results for the Taipei Basin.

In general, this study focused on forward simulation using the ETF-based site correction stochastic simulation technique to predict future disastrous earthquakes. In addition to using individual ETFs for each strong motion stations for discussing the accuracy of prediction errors in the next section, the average ETF spectra for the Taipei Basin were checked first in order to ensure that the simulated VHR motion construction reflected the combination response of the source and path terms, and left the remaining site part in the ETF calculation. To calculate the average ETFs for the Taipei Basin, the stations located on the edge or the center of the basin were not classified into different groups. The correction of

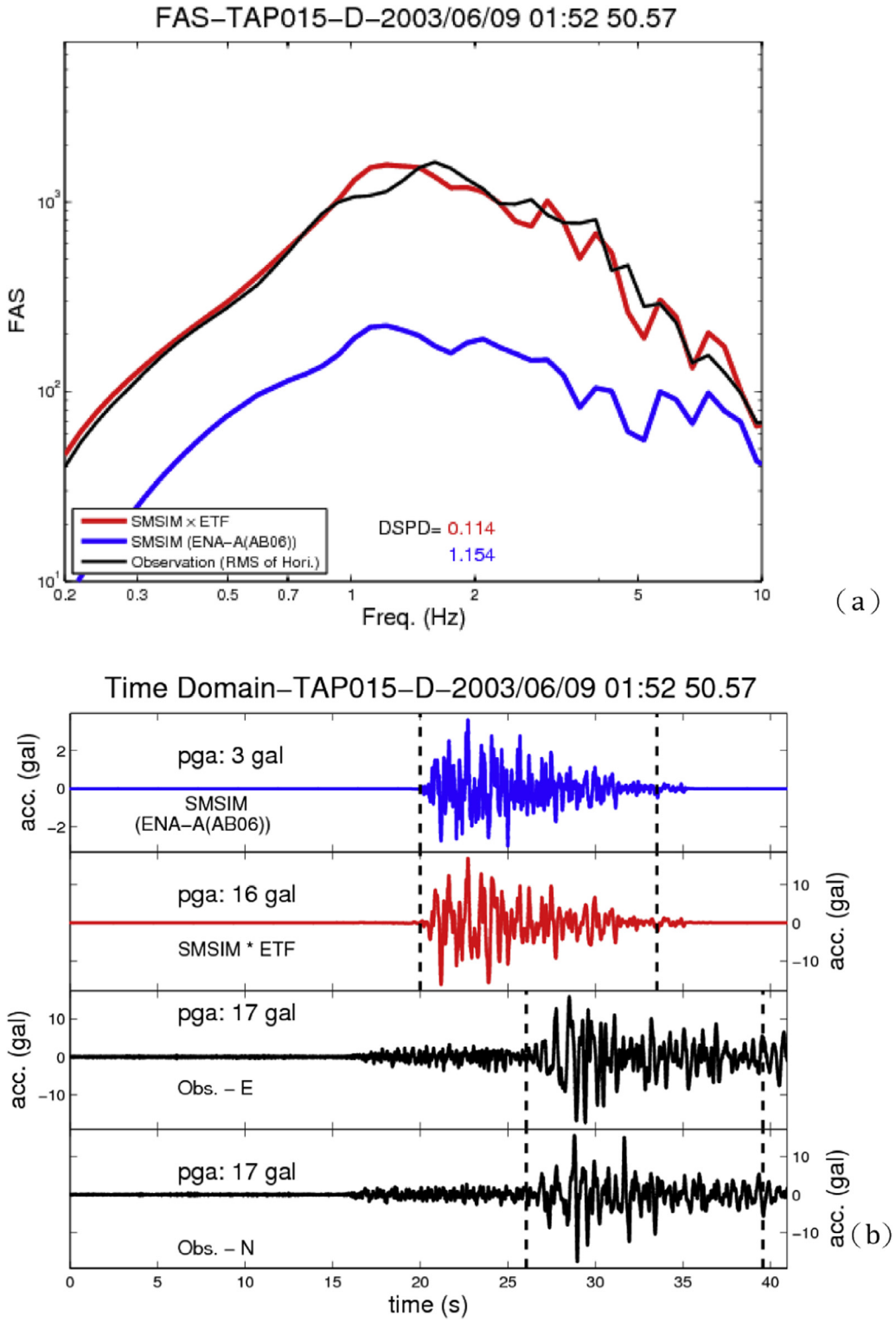

Fig. 7. Example of site correction of the ETF from the stochastic point source simulation (SMSIM). (a) Frequency domain; the blue line is the original simulation result based on VHR, the red line is the ETF correction results, and the black line is the observation record from target event 1. (b) Time domain of acceleration records; the dashed lines indicate windows of shear wave portion. (For interpretation of the references to colour in this figure legend, the reader is referred to the web version of this article.)

the average site motion will be easier to apply for individual sites within the basin where sufficiently strong motion records do not exist; therefore, site classification can be obtained using geophysics methods such as P-S logging measurements (Kuo et al., 2012) and microtremor arrays (Kuo et al., 2016). Future possible earthquake hazard mitigation in the basin would be efficient if the average ETFs are identical to those obtained using the traditional site response studies. For average ETFs, site class B shows that the amplification occurred with high frequency, indicating that thin sedimentary layers might have covered the rock sites in this region. In contrast, the high-frequency (5–10 Hz) responses of the ETFs in site classes C, D, and E indicate similar characteristics at low amplification. The dominant frequencies range from 0.5 to 2 Hz for classes D and E, which relate to the response of the Sungshan formation in the basin (Chen et al., 2016; Wang et al., 2004; Wen and Peng, 1998).

A contour plot of the dominant frequencies of the ETFs in the Taipei Basin is shown in Fig. 5. The distribution of dominant frequencies indicates that the region near the basin edge has a higher dominant frequency, while that within the basin has two lower dominant frequency zones. The distribution correlates with the soil layer thickness, and the lower dominant frequency zone occurs over the deepest part of the soil layer. The top soft soil layer, *i.e.*, the Sungshan formation, as indicated by previous studies (Wang

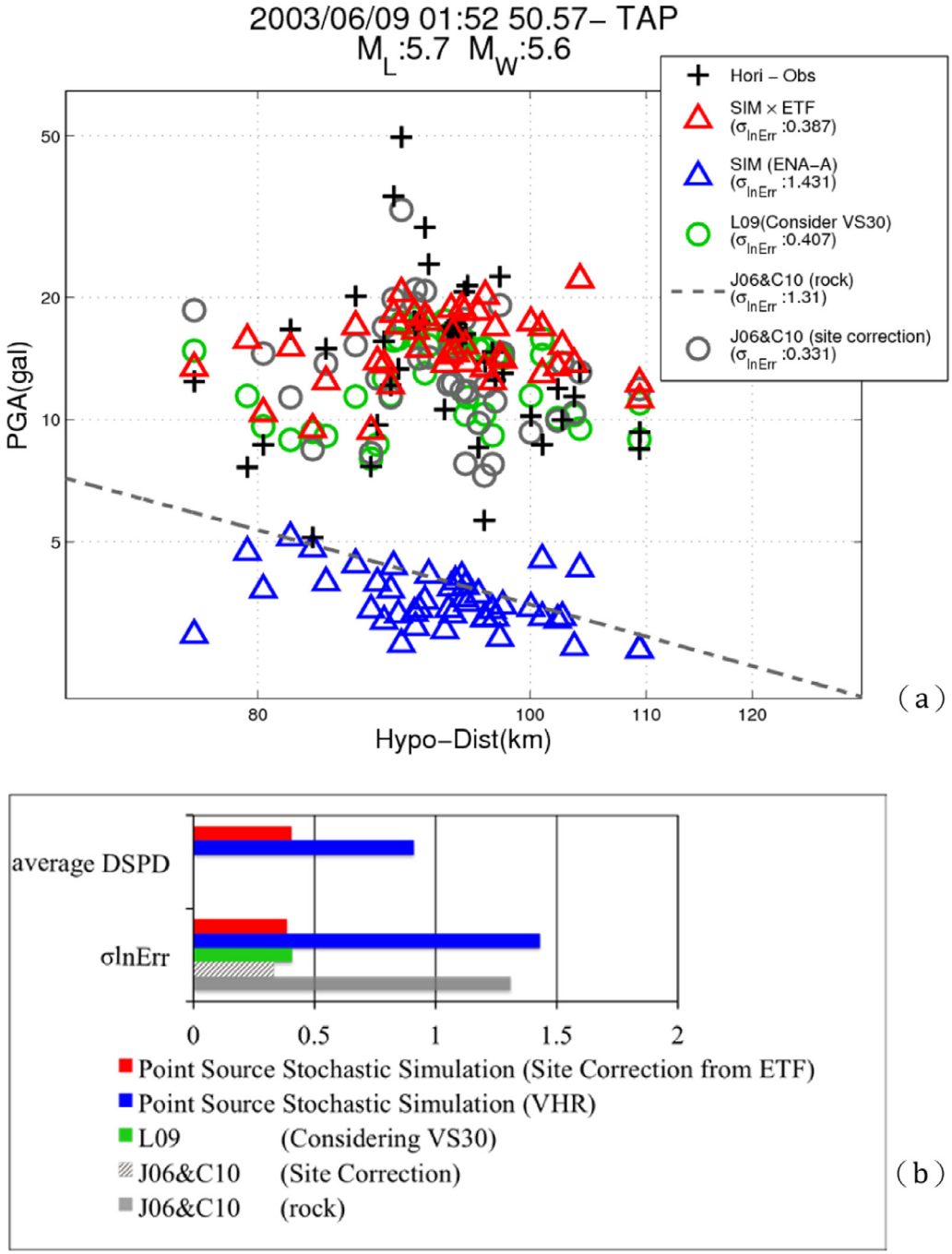

Fig. 8. Target event 1: (a) attenuation relation of the PGA from horizontal observation (black crosses), prediction after ETF site correction from the stochastic simulation (red triangles), stochastic simulation with VHR (blue triangles), GMPE (from L09) (green circles), rock GMPE (from J06&C10) (gray dashed line), site-corrected GMPE (from J06&C10) (gray circles). (b) Comparison of DSPDs in the frequency domain and $\sigma_{\ln Err}$ in the time domain for the different methods. (For interpretation of the references to colour in this figure legend, the reader is referred to the web version of this article.)

et al., 2004; Wen and Peng, 1998), within the Taipei Basin reacts to the site effects at low frequency, which agrees well with the results of this study. The individual ETF of a cross-section across the basin indicates that the dominant frequency is 0.2–1 Hz for the deeper part of the basin (westward part), and the range gradually increases to 1.5–3.5 Hz for the shallower part (eastward region). This indicates a specific difference in the site effects for each station within the basin. Furthermore, the amplification contours at 0.5 and 2.0 Hz of the ETF in the Taipei Basin (Fig. 6) show very clear hot spots of high amplification in two areas, the western and eastern parts of the Taipei Basin, for a 0.5-Hz response. These areas are also the deepest parts of the Sungshan formation. This amplification is most likely caused by the response of the soft soil layer and high impedance contrast between the layer and the underlying rock. However, the high-amplification area for the 2.0-Hz response shifts to the basin edge areas, except in the western part of the deep alluvium area. Similar assumptions were also made in a previous site effect study based on microtremor analysis in the Taipei Basin (Wen et al., 2006; Wen and Huang, 2012).

5. Results and discussions

After ETFs were calculated for each station, the forward strong motion simulation was applied individually through the following steps (Fig. 7): (1) The VHR spectrum was synthesized using the stochastic point-source simulation (blue line in Fig. 7(a)). (2) ETFs for individual stations were modified to the VHR simulation spectra (red line in Fig. 7(a)). 3) An inverse fast Fourier transformed was applied to convert the ETF-modified spectra back to the time domain using the phase of VHR simulation, and PGA was calculated (red time history in Fig. 7(b)).

The ETFs for each station were constructed using a database of shallow and small earthquakes, namely the calibration set of earthquakes (green circles in Fig. 1). To test and verify the site correction results in this study, three target earthquakes were selected as the validation set, which were not included in the calibration database; their locations are indicated by red stars in Fig. 1. The following are the seismic source parameters of these earthquakes. (1) A shallow, small earthquake that occurred off the coast of Hualian, Taiwan, at 01:52 on 9th June 2003 (UTC) (target event 1) with a magnitude of M_L = 5.6 and a focal depth of 23.2 km was selected as it fitted the conditions of the database for ETF construction. (2) A shallow, large earthquake that occurred at the northern end of the East Rift Valley, Taiwan, at 08:54 on 10th September 2000 (UTC) (target event 2) with a magnitude of M_L = 6.2 and a focal depth of 17.74 km; its magnitude was slightly larger than that in the database. (3) In contrast, a small (M_L = 5.5) but deep (depth 76 km) earthquake that occurred near the coast in Ilan, Taiwan, at 04:13 on 24th March 1995 (UTC) (target event 3) was selected.

The time domain and frequency domain errors were checked in this study using $\sigma_{\ln Err}$ and the degree of spectra difference (DSPD). The equations are as follows:

$$\sigma_{\ln Err} = \sqrt{\frac{1}{N}\sum_{i=1}^{N}(\ln Err_i)^2}, \text{ where} \tag{24}$$

$$\ln Err = \ln PGA_o - \ln PGA_{sim}, \tag{25}$$

N is the station number, PGA_O is the observed PGA with a geometric mean of two horizontal components, and PGA_{sim} is the simulated PGA. The area between the two spectra was calculated using the DSPD in the frequency domain, as follows:

$$DSPD = \sum_{i=0.2}^{10}\left(\left|\log_{10}\frac{FAS_o}{FAS_s}\right| \times df\right), \text{ where} \tag{26}$$

$$df = \log_{10}(f_{i+1}/f_i), \tag{27}$$

where FAS_O is the observed Fourier spectra, FAS_S is the simulated Fourier spectra, and df is the sampling frequency in the log scale. A frequency band of 0.2–10 Hz was considered as most of the dominant site effects were found to occur in this range. In addition,

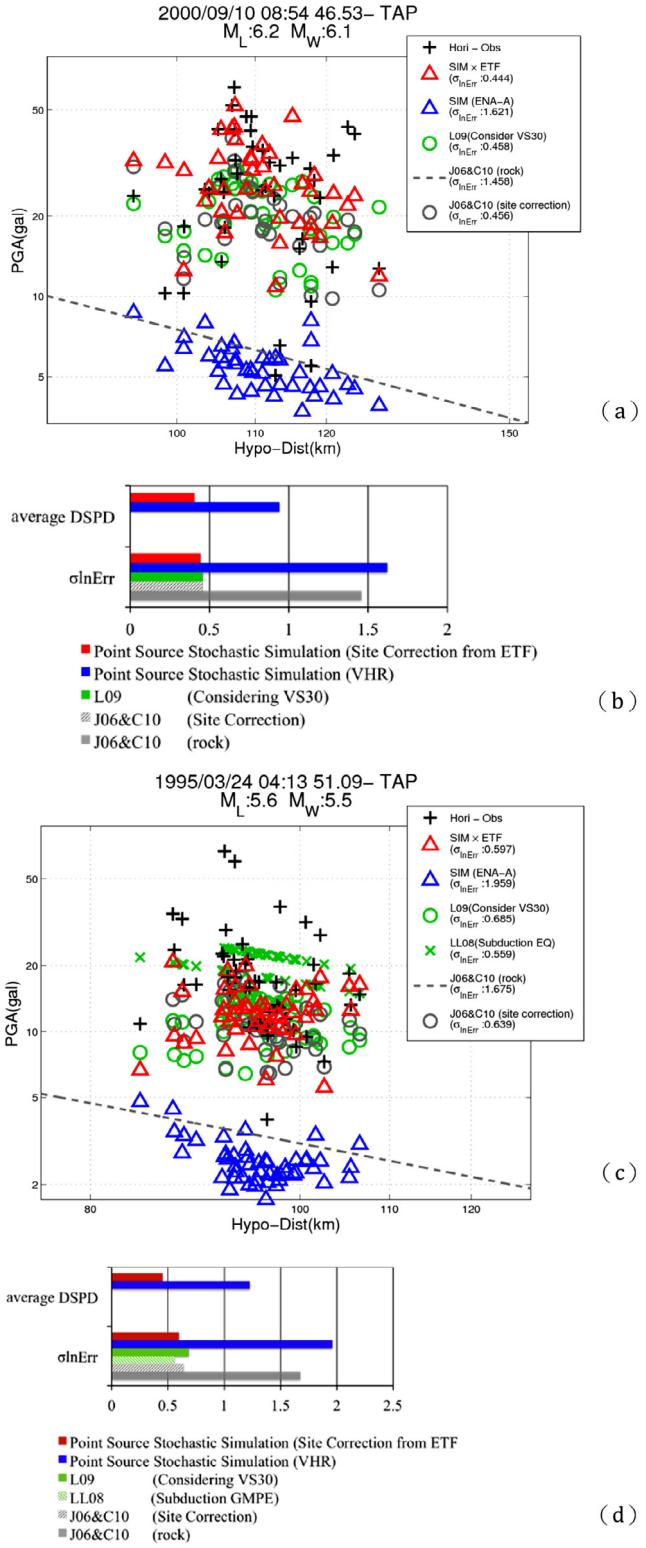

Fig. 9. Target event 2: (a) PGA attenuation relation and (b) comparisons of DSPD in the frequency domain and $\sigma_{\ln Err}$ in the time domain for different methods. Target event 3: (c) PGA attenuation relation and (d) comparisons of DSPD in the frequency domain and $\sigma_{\ln Err}$ in the time domain for different methods. The legend is the same as for Fig. 8.

the correlation coefficient r was used to check for similarity in the frequency domain.

Two different site corrections for the GMPE were compared with the predicted PGA_{sim} in this study. The first one is the two-stage attenuation equation (Jean et al., 2006; Chang et al., 2010; hereafter denoted as J06&C10). Rock site records were first regressed as follows:

$$Y_{att} = 0.00369e^{1.75377M}[R + 0.1222e^{0.78315M}]^{-2.05644}, \quad (28)$$

where Y_{att} is the predicted PGA (units: g), distance R is the shortest distance to the rupture fault plane (using the hypocentral distance if the fault plane cannot be found), and M is the local magnitude M_L. The unique linear relationship between the observation and first-stage prediction (Y_{att}) at each strong motion station at each soil site was used for the site correction of the GMPE. The regression equation is defined as follows:

$$\ln PGA_s = C_0 + C_1 \times \ln(Y_{att})_s, \quad (29)$$

where PGA_S is the observed PGA at the soil site station and $(Y_{att})_s$ is the first-stage prediction for the station. Each station will calculate one set of linear regression factors C_0 and C_1 to predict the second-stage PGA. The second GMPE used data for Taiwan and followed the procedure of the NGA, which considered V_S30 as a site correction term for the GMPE (Lin, 2009; hereafter denoted as L09). The equation is as follows:

$$\ln y = C_1 + F_1 + C_3(8.5 - M_w)^2 + (C_4 + C_5(M_w - 6.3)) \times \ln(\sqrt{R^2 + exp(H)^2}) + C_6F_{NM} + C_7F_{RV} + C_8 \times \ln(VS_{30}/1130), \text{ for} \quad (30)$$

$$\begin{cases} F_1 = C_2(M_w - 6.3), & M_w \leqslant 6.3 \\ F_1 = (-H \cdot C_5)(M_w - 6.3), & M_w > 6.3 \end{cases}, \quad (31)$$

where y is the predicted PGA (unit: g), C_1–C_8 are regression factors, H is the saturation term for the near field, the magnitude is M_w, R is the same distance as for Eq. (28), and F_{NM} and F_{RV} are fault-type terms to represent normal or reverse faults, respectively.

Table 2
Parameters for the 1999 Chi-Chi earthquake using the finite-fault simulation.

Magnitude (M_W)	7.6
Strike, Dip, Depth of Initial Rupture	5.0, 34.0, 0 (Chang et al., 2000)
Fault dimension	110 km × 40 km (Ma et al., 2001)
Subfault dimension	5 km × 5 km
Rupture velocity	0.8 β

In this study, the ETF is constructed and the abovementioned GMPE for shallow earthquakes is considered using the database of shallow earthquakes. However, deep earthquakes (target event 3) require another GMPE constructed for deep events. Thus, a subduction GMPE (Lin and Lee, 2008; hereafter denoted as LL08) for rock and soil sites was used for verification. For rock sites (sites B and C), the GMPE is:

$$\ln y = -2.5 + 1.205M - 1.905\ln(R + 0.516e^{0.6325M}) + 0.0075H_{hypo} + 0.275Z_t, \quad (32)$$

and for soil sites (site D and E), it is:

$$\ln y = -0.9 + 1.00M - 1.90\ln(R + 0.9918e^{0.5263M}) + 0.004H_{hypo} + 0.31Z_t, \quad (33)$$

where the magnitude is the moment magnitude M_w, R is the hypocentral distance, H_{hypo} is the focal depth, and $Z_t = 1$ means the subduction term will be considered.

Fig. 7 shows an example of ETF site correction from the stochastic simulation for target event 1. The DSPD shows a significant drop from 1.154 to 0.114 and r increases from 0.91 to 0.953 in the frequency domain, implying that the corrected spectra fit the horizontal observation very well. The PGA can also reach the same correction level as in the time domain, although the predicted time history still does not match the observed waveform, owing to the random phase setting in the stochastic simulation. In general, ETF site correction is a good approach for target event 1 and is suitable for a database of shallow and small earthquakes (Fig. 8). The time domain error $\sigma_{\ln Err}$ showed that site correction was needed for the simulation of VHR and the GMPE for a rock site. The ETF site correction results can reach the same level as the site-corrected GMPE. In addition, the average DSPD of the TSMIP stations in the Taipei Basin that recorded target event 1 improved from around 0.9 to 0.4 in the frequency domain. In contrast, the ETF site correction simulation is suitable for shallow earthquakes with slightly larger magnitudes (target event 2, Fig. 9(a) and (b)), but would not be suitable for deep earthquakes with small magnitudes, owing to the differences in the characteristics at different focal depths, although the DSPD results are still suitable (target event 3, Fig. 9 (c) and (d)). The LL08 equation was selected for a deep-earthquake GMPE, the aforementioned GMPEs (J06&C10, L09) use the shallow earthquake database; the LL08 equation gave a better prediction than the shallow GMPE and ETF site correction simulation, which indicating that a deep-event-based ETF would likely be needed for a deep target earthquake.

Finally, the finite-fault stochastic ground-motion simulation was applied to the 1999 Chi-Chi earthquake in Taiwan, owing to

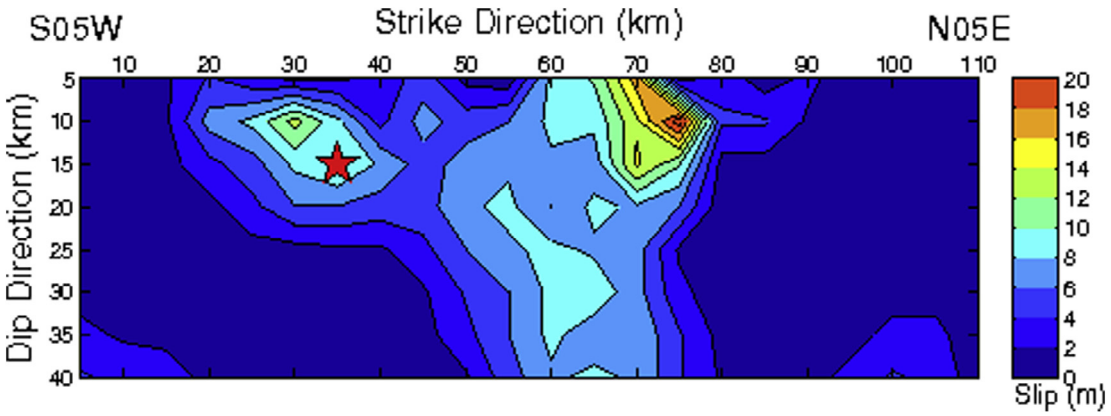

Fig. 10. Slip distribution of the Chelongpu fault during the 1999 Chi-Chi, Taiwan, earthquake. The star indicates the seismic source, and the fault strike is toward the N05E direction (redrawn from Ma et al., 2001).

the complexity of its fault rupture system. The basic source parameters of the point-source simulation listed in Table 1 were applied for the Chi-Chi earthquake and some were added for the finite-fault simulation (Table 2). A fault slip model with an asperity distribution calculation was adopted from Ma et al. (2001) and is shown in Fig. 10. Results of site correction for the stochastic finite-fault simulation using the ETF based on the database of shallow, small earthquakes (Fig. 11) show that the spectra were slightly overestimated in the high-frequency band (5–10 Hz), regardless of the site classification. This means the overestimating phenomenon was not due to site effects and might be because the energy contained in the high-frequency part is lower in a large earthquake, as greater low-frequency waves are generated from a longer rupture process. The ETF based on a shallow, small earthquake cannot totally reflect the response of a huge earthquake, but prediction errors including DSPD and $\sigma_{\ln Err}$ can be efficiently reduced (Fig. 12). The slightly higher PGA prediction results indicate that it is a conservative estimate of ground motion for disaster prevention purposes.

Whether the ground motion prediction must be performed using theoretical simulation techniques or by applying the GMPE is a topic of ongoing debate. This is because the GMPE uses a statistical-based regression process and deduces standard deviation from several physical effects, while a simulation technique such as the stochastic simulation first superposes physical effects step-by-step to compose a ground motion prediction. This means that if a theoretical method can provide a better or even similar prediction accuracy level compared with the level of the GMPE method, then the theoretical method can be considered to generate more confident predictions for future possible earthquakes.

In general, the results of PGA simulations from site correction using the ETF can provide the same level of prediction as the site-corrected GMPE (J06&C10) and can produce acceptable spectrum fitting results (Figs. 11 and 12). However, although strong site effects will induce an amplified strong ground motion in the Taipei Basin, which makes it a good example for discussing the effectiveness of site correction, the simulation in this study displayed only far-field behavior for the target Chi-Chi earthquake. This is because the geographic location of the Taipei Basin is over 150 km from the fault plane; therefore, the near-field response induced by the complex fault rupture geometry could not be discussed in this study.

Furthermore, considering forward ground motion simulation for future possible earthquake hazard mitigation is the main focus of this study, the selected stochastic simulation technique

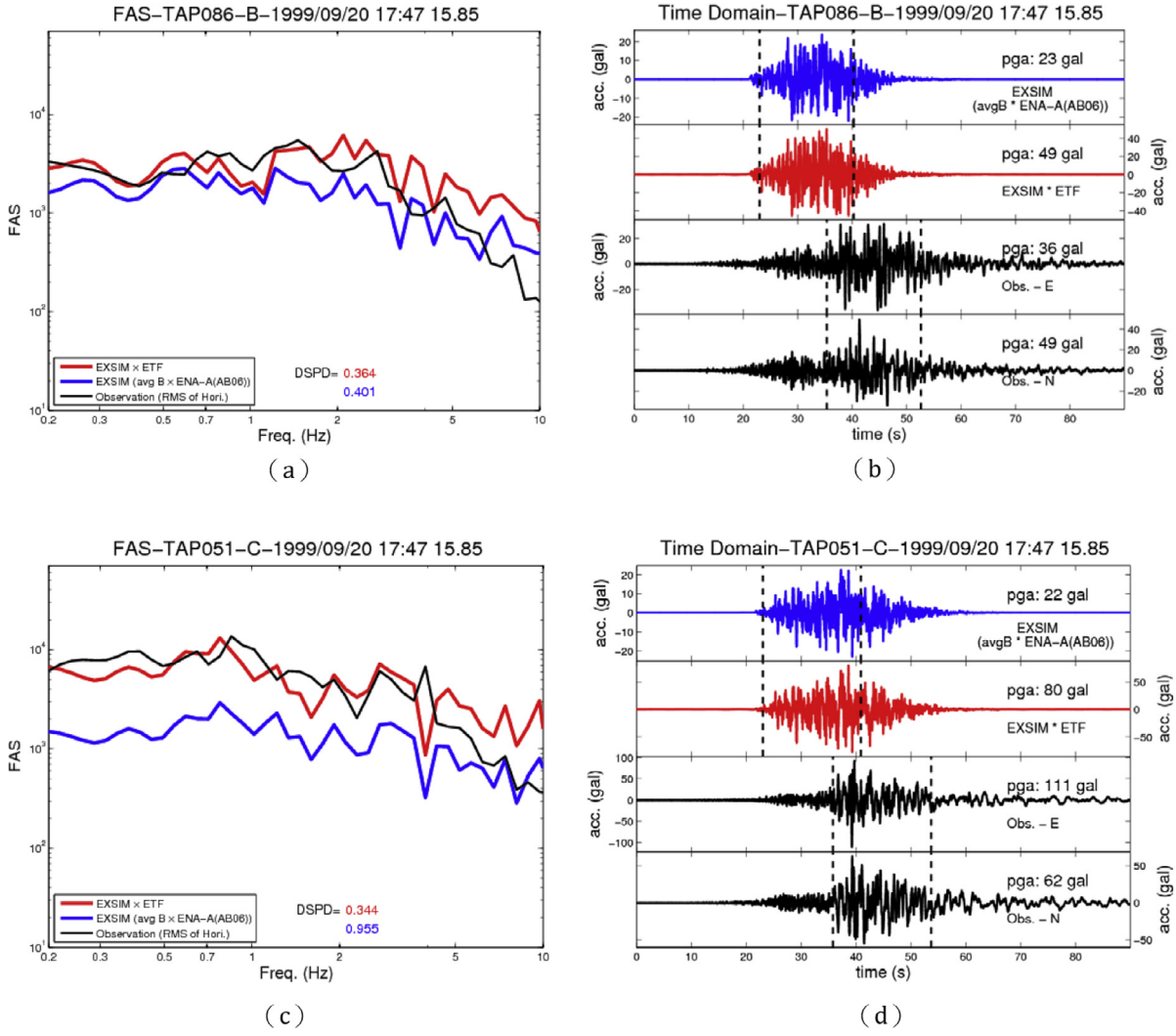

Fig. 11. Examples of ETF site correction for a stochastic finite-fault simulation of the 1999 Chi-Chi, Taiwan, earthquake with different site classes in the Taipei Basin: class B, Vs30 = 942.8 m/s, TAP086 in (a) frequency domain and (b) time domain; class C, Vs30 = 401.8 m/s, TAP051 in (c) frequency domain and (d) time domain.; class D, Vs30 = 200.6 m/s, TAP026 in (e) frequency domain and (f) time domain.; class E, Vs30 = 177.0 m/s, TAP005 in (g) frequency domain and (h) time domain. Legends are the same with Fig. 7.

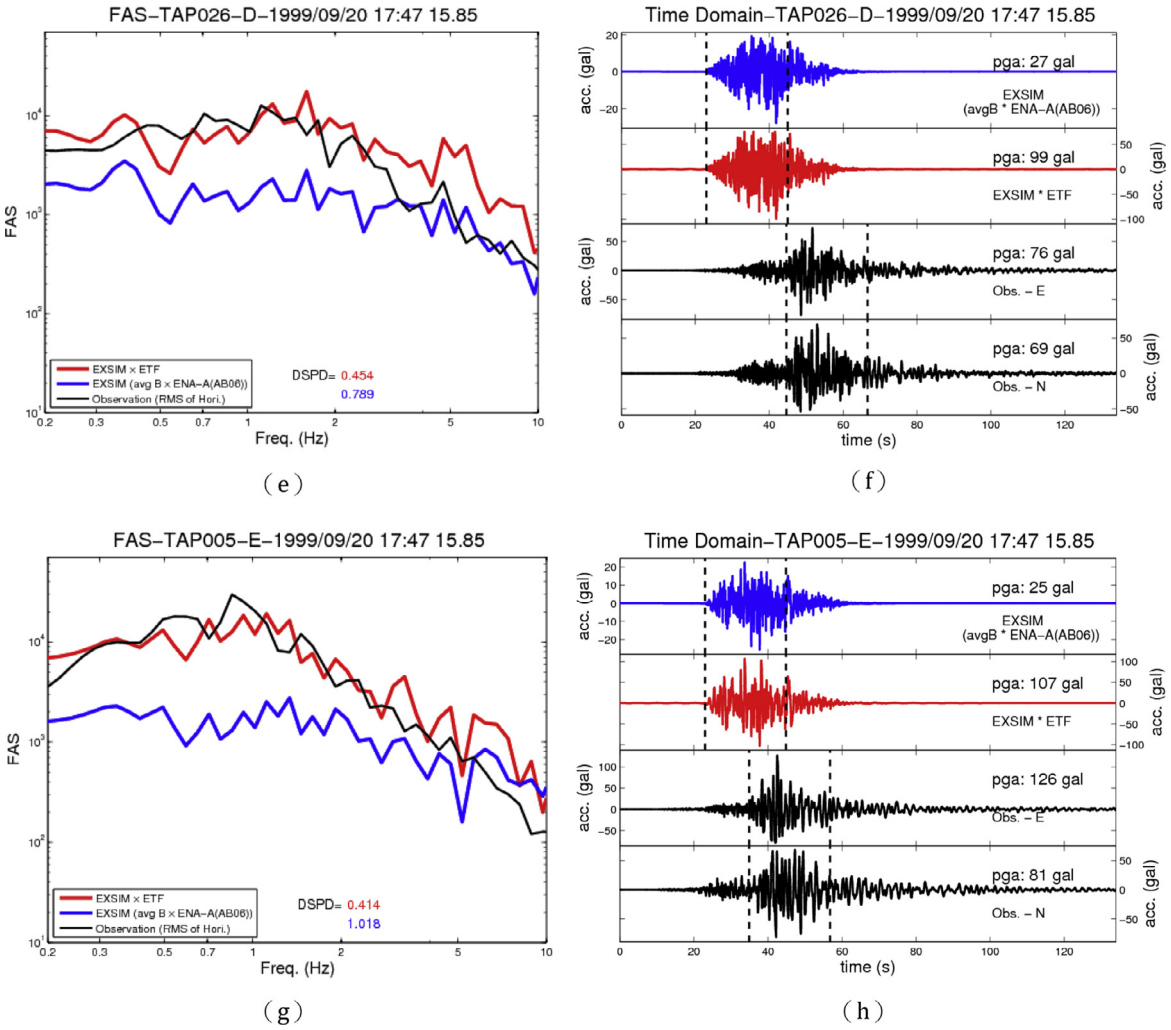

Fig. 11 (*continued*)

can provide physics-based high-frequency (at least to 10 Hz) Fourier spectra step by step using well-estimated parameter model settings, including source, path and site effects. Therefore, the VHR construction process in combination with the stochastic parameter settings obtained from three previous studies (Sokolov et al., 2009; D'Amico et al., 2012; Lee et al., 2015) for the Taiwan region was applied. As the parameters in the stochastic simulation are highly correlated with each other and there are trade-off issues in parameter determining process, the remaining prediction residuals (denoted as the ETF in this study) were mainly related to the local site responses. The ETF responses in the Taipei Basin exhibit a trend similar to that obtained in previous site effect studies, indicating that the ETF can be used for site correction of the stochastic point-source simulation method for soil sites. Meanwhile, it was also demonstrated that the ETF-based site correction method is suitable for large earthquakes, such as the Chi-Chi, Taiwan (Mw = 7.6) earthquake, by using finite-fault stochastic simulation with a proper slip asperity model in both PGA and Fourier amplitude spectra (FAS) predictions.

Finally, not only the frequency behavior but also PGA prediction was the main focus in this study. The conclusion indicates that PGA simulations for shallow events using the shallow ETF have effective prediction ability. The ETF-based site-corrected stochastic simulation can provide a similar accuracy level to the fully empirical GMPE. This implies that the abovementioned method provides a balance between theoretical and application purposes for the engineering seismological field. Finally, while the simulated errors of the ETF-corrected FAS and PGA can cover the epistemic uncertainty, aleatory uncertainty that may arises from the random phase setting for time history and unconfirmed factors remain for stochastic simulation.

6. Conclusions

In this study, empirical transfer functions (ETF) were constructed based on a point-source stochastic simulation and observations from a database of shallow (<30 km), small (M_w < 6.0) earthquakes from Taiwan Strong Motion Instrumentation Program stations in the Taipei Basin. The general ETF of the Taipei Basin indicated that the harder the soil at the site, the higher the dominant frequency of the response. The results fit the assumptions made in previous studies using observation data, which indicates that the parameters and the model used in the stochastic simulation in this study indeed fit the reference rock conditions in the Taipei Basin. Contour maps of the dominant frequency and amplification distribution also support these findings. From the contour map of the dominant frequency, the main response within the Taipei Basin was around 0.5–2 Hz. Amplification contours at 0.5 Hz clearly showed two hot spots (the yellow regions in Fig. 6(a), in

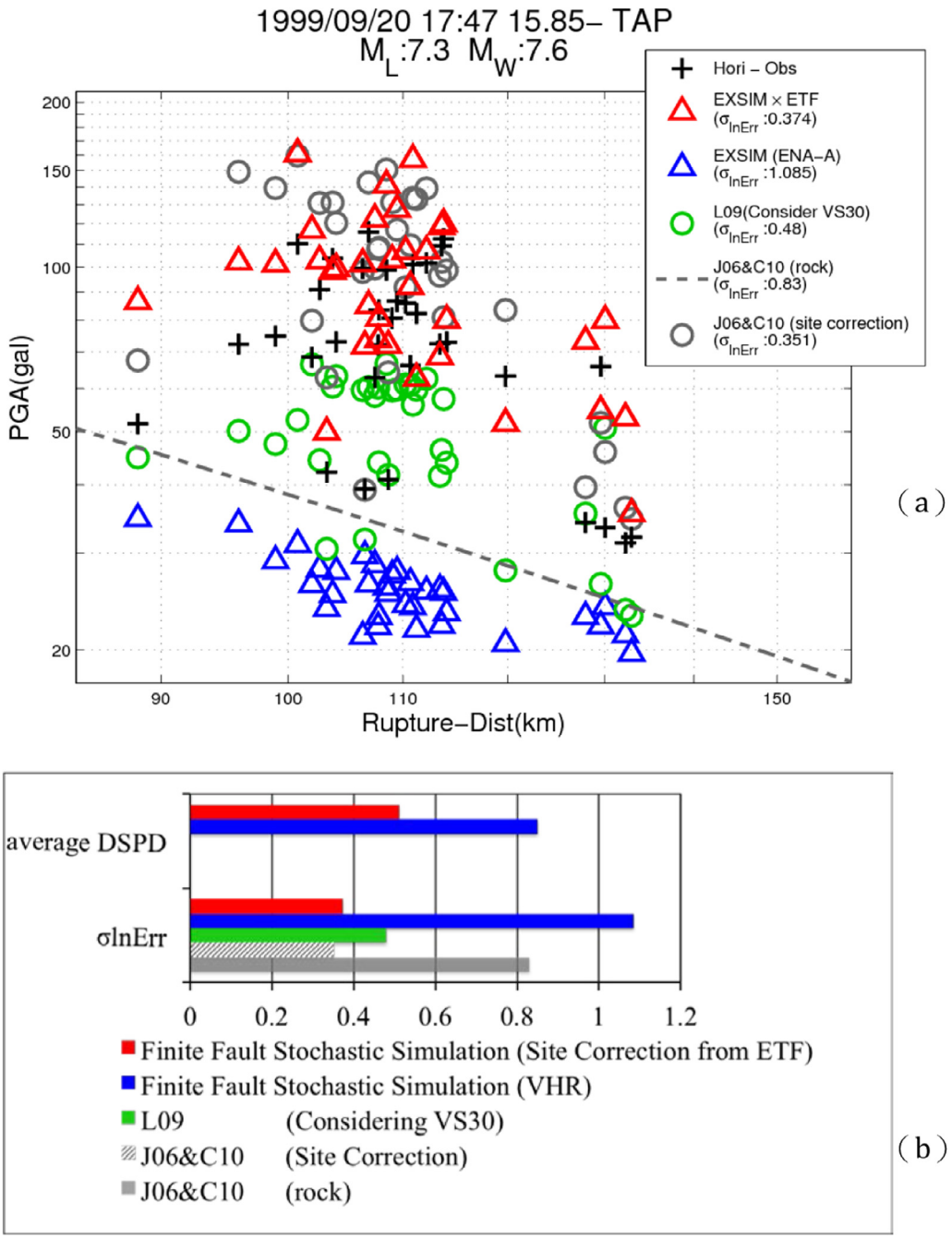

Fig. 12. (a) PGA attenuation relation for the 1999 Chi-Chi, Taiwan, earthquake. Rupture distance was used here for finite-fault results, and the fault geometry followed the results of a surface geological survey (the red line in Fig. 1). (b) Error comparisons in time and frequency domains. The legend is the same as in Fig. 8. (For interpretation of the references to colour in this figure legend, the reader is referred to the web version of this article.)

the western and eastern parts of the basin) of amplification that are related to the deepest part of the bottom of the Sungshan formation, which is the boundary of the engineering bedrock of the Taipei Basin.

Results of high-frequency predictions (0.2–10 Hz in this study) of the ETF-based site correction of the stochastic strong-motion simulation agreed well in both time and frequency domains when the depth and magnitude of the target earthquake belonged to the earthquake database. In addition, although the site correction function of the finite-fault simulation of the 1999 Chi-Chi, Taiwan, earthquake based on the ETF produced a slight overestimate in the high-frequency part, a conservative estimate can still be produced from the ETF-based site correction technique. The prediction level was the same as that of the site-corrected ground-motion prediction equation. This means that a theoretical calculation of strong ground motion, regardless of the peak ground acceleration or frequency domain, can aid advance planning of disaster prevention for individual fault systems in the future.

7. Data and resources

The fortran based source code SMSIM and EXSIM was downloaded from Dr. David Boore's personal website (http://www.daveboore.com/software_online.html, last accessed June 2016). Program version of SMSIM and EXSIM are 3.400 and 2011.11.22

respectively, with some modifications were described in this manuscript. The seismic waveform data of Taipei station was from TSMIP database that was belong to CWB. The site classification and V_S30 information of Taipei station were obtained from the Engineering Geological Database for TSMIP (EGDT; http://egdt.ncree.org.tw, last accessed June 2016).

Acknowledgments

This work was supported by the National Science Council, Taiwan [grant numbers NSC 101-2116-M-008-021, NSC 102-2116-M-008-023]. Appreciation is extended to the Central Weather Bureau, Taiwan for providing TSMIP earthquake data.

References

Abrahamson, N., Atkinson, G.M., Boore, D.M., Bozorgnia, Y., Campbell, K.W., Chiou, B.S.J., Idriss, I.M., Silva, W., Youngs, R., 2008. Comparisons of the NGA ground-motion relations. Earthquake Spectra 24 (1), 45–66.

Aki, K., 1967. Scaling law of seismic spectrum. J. Geophys. Res. 72 (4), 1217–1231.

Anderson, J.G., Hough, S.E., 1984. A model for the shape of the Fourier amplitude spectrum of acceleration at high frequencies. Bull. Seismol. Soc. Am. 74 (5), 1969–1993.

Atkinson, G.M., 1995. Attenuation and source parameters of earthquakes in the Cascadia region. Bull. Seismol. Soc. Am. 85 (5), 1327–1342.

Atkinson, G.M., 1996. The high-frequency shape of the source spectrum for earthquakes in eastern and western Canada. Bull. Seismol. Soc. Am. 86 (1A), 106–112.

Atkinson, G.M., Silva, W., 1997. An empirical study of earthquake source spectra for California earthquakes. Bull. Seismol. Soc. Am. 87 (1), 97–113.

Atkinson, G.M., Boore, D.M., 1998. Evaluation of models for earthquake source spectra in Eastern North America. Bull. Seismol. Soc. Am. 88 (4), 917–934.

Atkinson, G.M., Boore, D.M., 2006. Earthquake ground-motion prediction equations for eastern north America. Bull. Seismol. Soc. Am. 96 (6), 2181–2205.

Atkinson, G.M., Beresnev, I.A., 2002. Ground motions at Memphis and St. Louis from M 7.5–8.0 earthquakes in the New Madrid seismic zone. Bull. Seismol. Soc. Am. 92 (3), 1015–1024.

Beresnev, I.A., Atkinson, G.M., 1997. Modeling finite-fault radiation from the ω^n spectrum. Bull. Seismol. Soc. Am. 87 (1), 67–84.

Beresnev, I.A., Atkinson, G.M., 1998a. FINSIM – a FORTRAN program for simulating stochastic acceleration time histories from finite faults. Seismol. Res. Lett. 69 (1), 27–32.

Beresnev, I.A., Atkinson, G.M., 1998b. Stochastic finite-fault modeling of ground motions from the 1994 Northridge, California earthquake. I. Validation on rock sites. Bull. Seismol. Soc. Am. 88 (6), 1392–1401.

Boore, D.M., 1983. Stochastic simulation of high-frequency ground motions based on seismological models of the radiated spectra. Bull. Seismol. Soc. Am. 73 (6), 1865–1894.

Boore, D.M., 2003. Simulation of ground motion using the stochastic method. Pure Appl. Geophys. 160, 635–676.

Boore, D.M., 2009. Comparing stochastic point-source and finite-source ground-motion simulations: SMSIM and EXSIM. Bull. Seismol. Soc. Am. 99 (6), 3202–3216.

Boore, D.M., Atkinson, G.M., 2008. Ground-motion prediction equations for the average horizontal component of PGA, PGV, and 5%-damped PSA at spectral periods between 0.01 s and 10.0 s. Earthquake Spectra 24 (1), 99–138.

Boore, D.M., Joyner, W.B., 1982. The empirical prediction of ground motion. Bull. Seismol. Soc. Am. 72 (6), S43–S60.

Boore, D.M., Joyner, W.B., 1997. Site amplifications for generic rock sites. Bull. Seismol. Soc. Am. 87 (2), 327–341.

Boore, D.M., Joyner, W.B., Wennerberg, L., 1992. Fitting the stochastic ω^2 source model to observed response spectra in western north America: Trade-offs between $\Delta\sigma$ and κ. Bull. Seismol. Soc. Am. 82 (4), 1956–1963.

Boore, D.M., Thompson, E.M., 2014. Path duration for use in the stochastic-method simulation of ground motions. Bull. Seismol. Soc. Am. 104 (5), 2541–2552.

Brune, J.N., 1970. Tectonic stress and the spectra of seismic shear waves from earthquake. J. Geophys. Res. 75 (26), 4997–5009.

Campbell, K.W., Bozorgnia, Y., 2008. NGA ground motion model for the geometric mean horizontal component of PGA, PGV, PGD and 5% damped linear elastic response spectra for periods ranging from 0.01 to 10 s. Earthquake Spectra 24 (1), 139–171.

Chandler, A.M., Lam, N.T.K., Tsang, H.H., 2006. Regional and local factors in attenuation modelling: Hong Kong case study. J. Asian Earth Sci. 27, 892–906.

Chang, C.H., Wu, Y.M., Shin, T.C., Wang, C.Y., 2000. Relocation of the 1999 Chi-Chi earthquake in Taiwan. Terrestrial, Atmospheric Oceanic Sci. 11 (3), 581–590.

Chang, Y.W., Jean, W.Y., Chiu S.B., 2010. Study on the design earthquakes for Kinmen, Matsu and Penhu areas. Technical Report of National Center for Research Earthquake Engineering, report number NCREE-10-016 (in Chinese with English abstract).

Chen, K.C., 2003. Strong ground motion and damage in the Taipei basin from the Moho reflected seismic waves during the March 31, 2002, Hualien, Taiwan earthquake. Geophys. Res. Lett. 30 (11), 1551.

Chen, K.C., Shin, T.C., Wang, J.H., 1989. Estimates of coda Q in Taiwan. Proc. Geol. Soc. China 32, 339–353.

Chen, Y.C., Huang, H.C., Wu, C.F., 2016. Site-effect estimations for Taipei Basin based on shallow S-wave velocity structures. J. Asian Earth Sci. 117, 135–145.

Cheng, S.N., Wang, Z.B., Lin, Z.W., Chiang, C.H., 2010. Constructed seismic catalog in Taiwan region (II). Technique Report of Central Weather Bureau 57, 483–502 (in Chinese with English abstract).

Chiou, B.S.J., Youngs, R.R., 2008. An NGA model for the average horizontal component of peak ground motion and response spectra. Earthquake Spectra 24 (1), 173–215.

D'Amico, S., Akinci, A., Malagnini, L., 2012. Predictions of high-frequency ground-motion in Taiwan based on weak motion data. Geophys. J. Int. 189, 611–628.

Douglas, J., 2003. Earthquake ground motion estimation using strong-motion records: a review of equations for the estimation of peak ground acceleration and response spectral ordinates. Earth Sci. Rev. 61, 43–104.

Frankel, A., Mueller, C., Barnhard, T., Perkins, D., Leyendecker, E., Dickman, N., Hanson, S., Hopper, M., 1996. National seismic hazard maps: documentation June 1996. Open-File Reports U.S. Geological Survey 96–532.

Fletcher, J.B., Wen, K.L., 2005. Strong ground motion in the Taipei basin from the 1999 Chi-Chi, Taiwan, earthquake. Bull. Seismol. Soc. Am. 95 (4), 1428–1446.

Hanks, T.C., 1982. fMAX. Bull. Seismol. Soc. Am. 72 (6), 1867–1879.

Hung, T.V., Kiyomiya, O., 2013. Use of the stochastic-source model to simulate ground motion and response spectra in northern Vietnam. J. Asian Earth Sci. 62, 485–500.

Irikura, K., 1983. Semi-empirical estimation of strong ground motions during large earthquakes. Bulletin Disaster Prevent. Res. Inst. (Kyoto University) 33 (298), 63–104.

Irikura, K., 1986. Prediction of strong acceleration motions using empirical green's function. In: Proceedings of the 7th Japan Earthquake Engineering Symposium, Tokyo, pp. 151–156.

Irikura, K., Miyake, H., 2011. Recipe for predicting strong ground motion from crustal earthquake scenarios. Pure Appl. Geophys. 168, 85–104.

Jean, W.Y., Chang, Y.W., Wen, K.L., Loh, C.H., 2006. Early estimation of seismic hazard for strong earthquakes in Taiwan. Nat. Hazards 37, 39–53.

Ktenidou, O.J., Cotton, F., Abrahamson, N.A., Anderson, J.G., 2014. Taxonomy of κ: a review of definitions and estimation approaches targeted to applications. Seismol. Res. Lett. 85 (1), 135–146.

Kuo, C.H., Wen, K.L., Hsieh, H.H., Lin, C.M., Chang, T.M., Kuo, K.W., 2012. Site classification and Vs30 estimation of free-field TSMIP stations using the logging data of EGDT. Eng. Geol. 129–130, 68–75.

Kuo, C.H., Chen, C.T., Lin, C.M., Wen, K.L., Huang, J.Y., Chang, S.C., 2016. S-wave velocity structure and site effect parameters derived from microtremor arrays in the Western Plain of Taiwan. J. Asian Earth Sci. 128, 27–41.

Kurahashi, S., Irikura, K., 2011. Source model for generating strong ground motions during the 2011 off the Pacific coast of Tohoku earthquake. Earth Planets Space 63, 571–576.

Lee, S.J., Chen, H.W., Huang, B.S., 2008a. Simulations of strong ground motion and 3D amplification effect in the Taipei basin by using a composite grid finite-difference method. Bull. Seismol. Soc. Am. 98 (3), 1229–1242.

Lee, S.J., Chen, H.W., Liu, Q., Komatitsch, D., Huang, B.S., Tromp, J., 2008b. Three-dimensional simulations of seismic-wave propagation in the Taipei basin with realistic topography based upon the spectral-element method. Bull. Seismol. Soc. Am. 98 (1), 253–264.

Lee, Y.T., Ma, K.F., Wang, Y.J., Wen, K.L., 2015. An empirical equation of effective shaking duration for moderate to large earthquakes. Nat. Hazards 75 (2), 1779–1793.

Lin, P.S., Lee, C.T., 2008. Ground-motion attenuation relationships for subduction-zone earthquakes in northeastern Taiwan. Bull. Seismol. Soc. Am. 98 (1), 220–240.

Lin, P.S., 2009. Ground-Motion Attenuation Relationship and Path-Effect Study using Taiwan Data Set phD thesis. National Central University, Taiwan (in Chinese with English Abstract).

Ma, K.F., Mori, J., Lee, S.J., Yu, S.B., 2001. Spatial and temporal distribution of slip for the 1999 Chi-Chi, Taiwan, earthquake. Bull. Seismol. Soc. Am. 91 (5), 1069–1087.

Mayeda, K., Malagnini, L., 2009. Apparent stress and corner frequency variations in the 1999 Taiwan (Chi-Chi) sequence: evidence for a step-wise increase at Mw ~ 5.5. Geophys. Res. Lett. 36, L10308.

Miksat, J., Wen, K.L., Wenzel, F., Sokolov, V., Chen, C.T., 2010. Numerical modeling of ground motion in the Taipei basin: basin and source effects. Geophys. J. Int. 183, 1633–1647.

Miyake, H., Iwata, T., Irikura, K., 2003. Source characterization for broadband ground-motion simulation: kinematic heterogeneous source model and strong motion generation area. Bull. Seismol. Soc. Am. 93 (6), 2531–2545.

Motezedian, D., Atkinson, G.M., 2005. Stochastic finite-fault modeling based on a dynamic corner frequency. Bull. Seismol. Soc. Am. 95 (3), 995–1010.

National research Institute for Earth science and Disaster prevention (NIED), 2009. Strong ground motion prediction method ("Recipe") for earthquakes with specified source faults. Technical Note of NIED 336, Appendix 1–50.

Roumelioti, Z., Beresnev, I.A., 2003. Stochastic finite-fault modeling of ground motions from the 1999 Chi-Chi, Taiwan, earthquake: application to rock and

soil sites with implications for nonlinear site response. Bull. Seismol. Soc. Am. 93 (4), 1691–1702.
Saragoni, G.R., Hart, G.C., 1974. Simulation of artificial earthquakes. Earthquake Eng. Struct. Dynam. 2, 249–267.
Siddiqqi, J., Atkinson, G., 2002. Ground motion amplification at rock sites across Canada, as determined from the horizontal-to-vertical component ratio. Bull. Seismol. Soc. Am. 92 (2), 877–884.
Sokolov, V., 2000. Spectral parameters of ground motion in different regions: comparison of empirical models. Soil Dynam. Earthquake Eng. 19, 173–181.
Sokolov, V., Loh, C.H., Wen, K.L., 2000. Empirical model for estimating Fourier amplitude spectra of ground acceleration in Taiwan region. Earthquake Eng. Struct. Dynam. 29, 339–357.
Sokolov, V., Loh, C.H., Wen, K.L., 2001. Site-dependent design input ground motion estimations for the Taipei area: a probabilistic approach. Probab. Eng. Mech. 16, 177–191.
Sokolov, V., Loh, C.H., Wen, K.L., 2003. Evaluation of hard rock spectral models for the Taiwan region on the basis of the 1999 Chi-Chi earthquake data. Soil Dynam. Earthquake Eng. 23, 715–735.
Sokolov, V., Loh, C.H., Jean, W.Y., 2006. Strong ground motion source scaling and attenuation models for earthquakes located in different source zones in Taiwan. In: Proceedings of the 4th International Conference on Earthquake Engineering (4ICEE),12–13 October, Taipei, Taiwan, 4ICEE-0003.
Sokolov, V., Wen, K.L., Miksat, J., Wenzel, F., Chen, C.T., 2009. Analysis of Taipei basin response for earthquakes of various depths and locations using empirical data. Terrestrial, Atmospheric Oceanic Sci. 20 (5), 687–702.
Sun, X.D., Tao, X.X., Duan, S.S., Liu, C.Q., 2013. Kappa (k) derived from accelerograms recorded in the 2008 Wenchuan mainshock, Sichuan, China. J. Asian Earth Sci. 73, 306–316.
Tsai, C.C.P., 1997. Relationships of seismic source scaling in the Taiwan region. Terrestrial, Atmospheric Oceanic Sci. 8 (1), 49–68.
Tsai, K.C., Hsiao, C.P., Bruneau, M., 2000. Overview of building damages in 921 Chi-Chi earthquake. Earthquake Eng. Eng. Seismol. 2 (1), 93–108.
Tsai, Y.B., Lee, C.P., 2005. Strong motion instrumentation programs in Taiwan, directions in strong motion instrumentation. Nato Sci. Series: IV: Earth Environ. Sci. 58, 255–278.
Wang, C.Y., Lee, Y.H., Ger, M.L., Chen, Y.L., 2004. Investigating subsurface structures and P- and S-wave velocities in the Taipei basin. Terrestrial, Atmospheric Oceanic Sci. 15 (4), 609–627.
Wang, J.H., 1993. Q values of Taiwan: a review. J. Geol. Soc. China 36 (1), 15–24.
Wen, K.L., Chang, T.M., Lin, S.C., Lin, C.M., 2006. Site effect analysis from dense microtremor survey in the Taipei basin. In: Proceedings of the 4th International Conference on Earthquake Engineering (4ICEE), 12–13 October, Taipei, Taiwan, 4ICEE-0021.
Wen, K.L., Fei, L.Y., Peng, H.Y., Liu, C.C., 1995. Site effect analysis from the records of the Wuku downhole array. Terrestrial, Atmospheric Oceanic Sci. 6 (2), 285–298.
Wen, K.L., Huang, J.Y., 2012. Dense microtremor survey for site effect study in Taiwan. In: Proceedings of the 15th World Conference of Earthquake Engineering (15WCEE), 24–28 September, Lisbon, WCEE2012_1682.
Wen, K.L., Peng, H.Y., 1998. Site effect analysis in the Taipei basin: results from TSMIP network data. Terrestrial, Atmospheric Oceanic Sci. 9 (4), 691–704.